



Title	Spatial changes in the summer diatom community of the northern Bering Sea in 2017 and 2018
Author(s)	Fukai, Yuri; Abe, Yoshiyuki; Matsuno, Kohei et al.
Citation	Deep Sea Research Part II Topical Studies in Oceanography, 181-182, 104903 <a href="https://doi.org/10.1016/j.dsr2.2020.104903">https://doi.org/10.1016/j.dsr2.2020.104903</a>
Issue Date	2020-12
Doc URL	<a href="https://hdl.handle.net/2115/87787">https://hdl.handle.net/2115/87787</a>
Rights	© 2020. This manuscript version is made available under the CC-BY-NC-ND 4.0 license
Rights(URL)	<a href="https://creativecommons.org/licenses/by-nc-nd/4.0/">https://creativecommons.org/licenses/by-nc-nd/4.0/</a>
Type	journal article
File Information	Fukai et al. Manuscript.pdf



1 **Spatial changes in the summer diatom community of the northern**  
2 **Bering Sea in 2017 and 2018**

3  
4 Yuri Fukai<sup>a,\*</sup>, Yoshiyuki Abe<sup>b,c</sup>, Kohei Matsuno<sup>a,d</sup>, Atsushi Yamaguchi<sup>a,d</sup>

5  
6 <sup>a</sup>*Faculty/Graduate School of Fisheries Sciences, Hokkaido University, 3-1-1 Minato-cho, Hakodate,*  
7 *Hokkaido 041-8611, Japan*

8 <sup>b</sup>*Atmosphere and Ocean Research Institute, The University of Tokyo, 5-1-5, Kashiwanoha, Kashiwa-shi,*  
9 *Chiba, 277-8564, Japan*

10 <sup>c</sup>*Research Development Section, Office for Enhancing Institutional Capacity, Hokkaido University, Kita 21,*  
11 *Nishi 10, Kita-ku, Sapporo, Hokkaido, 001-0021, Japan*

12 <sup>d</sup>*Arctic Research Center, Hokkaido University, Kita-21 Nishi-11 Kita-ku, Sapporo, Hokkaido, 001-0021,*  
13 *Japan*

14 † Present address: *Division of Earth System Science, Graduate School of Environmental Science, Hokkaido*  
15 *University, Kita-10 Nishi-5 Kita-ku, Sapporo, Hokkaido, 060-0810, Japan*

16  
17 \* Corresponding author, Tel: 81-11-706-2246, Fax: 81-11-706-2247

18 *E-mail address:* [fukai@ees.hokudai.ac.jp](mailto:fukai@ees.hokudai.ac.jp) (Y. Fukai)

19  
20  
21 **ABSTRACT**

22  
23 In recent years, the northern Bering Sea has experienced changes in the timing of sea-ice  
24 retreat and in hydrographic conditions during the summer. The influence of these  
25 environmental changes on the diatom community has not been examined. In this study,

26 we investigated the spatial changes in the diatom community of the northern Bering Sea  
27 during the summers of 2017 and 2018, and evaluated the effects of environmental  
28 variability on these communities. We found that the diatom cell density and diversity  
29 varied with water masses. A cluster analysis based on cell density revealed that the diatom  
30 communities were separated into four groups, and that the distributions of three of these  
31 groups were different spatially between 2017 and 2018. In the Bering Strait and the  
32 Chirikov Basin regions, the diatom communities differed between 2017 and 2018. In  
33 2017, these diatom communities were dominated by cold-water species such as  
34 *Chaetoceros gelidus* and *Chaetoceros* spp. (subgenus *Hyalochaetae*), while in 2018, the  
35 community was dominated by cosmopolitan species such as *Thalassionema nitzschioides*  
36 and *Chaetoceros* spp. (subgenus *Phaeoceros*). NMDS and multiple regression analysis  
37 indicated that the timing of the sea-ice retreat was the most important contributor to the  
38 differences in the diatom community. In contrast, there was no year-to-year difference  
39 south of St. Lawrence Island, possibly because nutrients were depleted and phytoplankton  
40 types other than diatoms were dominant.

41

42 *Keywords:* Northern Bering Sea, Phytoplankton community, Diatoms, Year-to-year  
43 changes

44

## 45 **1. Introduction**

46           The northern Bering Sea is one of the most productive ocean regions in the world  
47 (Springer and McRoy, 1993). Supported by the high primary production, the area is  
48 important for higher trophic level species such as sea birds and marine mammals  
49 (Springer et al., 1996). This region is now facing drastic changes in sea-ice cover and  
50 hydrographic conditions during summer (Grebmeier et al., 2015; Frey et al., 2018). For  
51 example, reduced sea-ice cover in 2018 resulted in a diminished deep cold pool ( $< 2\text{ }^{\circ}\text{C}$ )  
52 south of St. Lawrence Island, and groundfish from the southeastern Bering Sea shifted  
53 northward., while the abundance of arctic species decreased in the region (Cornwall,  
54 2019; Duffy-Anderson et al., 2019). Given that sea-ice reduction is known to have  
55 affected some components of the northern Bering Sea, investigation of other components  
56 is required to understand the effects of future changes (Huntington et al., 2020).

57           The northern Bering Sea is a shallow shelf region. This region has a complicated  
58 hydrographic environment due to the inflow of multiple currents with different  
59 hydrographic features. The mixing of these waters results in complex hydrographic  
60 environments that affect the distribution of phytoplankton communities (Giesbrecht et al.,  
61 2019). In the northern Bering Sea, phytoplankton supports a high level of primary  
62 production in the upper mixed layer; most of this production settles to the seafloor due to  
63 low zooplankton grazing pressure (Grebmeier et al., 1988).

64           Diatoms play an important role as primary producers in high latitude marine  
65 ecosystems. A large diatom bloom occurs in the northern Bering Sea from the late spring  
66 to early summer, when the sea ice is melting and the light limit is diminishing; the  
67 chlorophyll *a* concentration can exceed  $8\text{ }\mu\text{g L}^{-1}$  during these blooms (Springer and  
68 McRoy, 1993). During the spring Arctic bloom, *Chaetoceros gelidus* sometimes

69 dominates (von Quillfeldt, 2000; Sergeeva et al., 2010). The composition of diatom  
70 communities varies among the different hydrographic environments (Taniguchi et al.,  
71 1976; Sergeeva et al., 2010). Diatoms constitute an important taxon in this marine  
72 ecosystem and require evaluation to understand how they respond to environmental  
73 change.

74           From 1978 to 2012, the timing of the sea-ice retreat (TSR) south of St. Lawrence  
75 Island, in the Chirikov Basin and in the Chukchi Sea has become earlier (Grebmeier et  
76 al., 2015; Frey et al., 2018). In the northern Bering Sea, the magnitude and timing of the  
77 phytoplankton bloom varies with the timing of the spring sea - retreat (Fujiwara et al.,  
78 2016). In 2018, the TSR was approximately two weeks earlier than it was during the  
79 previous year; the magnitude of the ice algal bloom was small and zooplankton abundance  
80 decreased (Cornwall, 2019; Fukai et al., 2019). However, despite the importance of  
81 diatoms for primary production, there is no information on how the diatom community  
82 responds to changes in sea-ice dynamics in the northern Bering Sea.

83           The purpose of our paper is to examine the phytoplankton communities,  
84 particularly with a focus on the diatom communities of the northern Bering Sea from  
85 62°N to the Bering Strait. To this end, we describe the species composition of diatoms,  
86 and test three hypotheses: 1) that the cell density and species composition of the diatom  
87 community differ by water mass, 2) that the diatom community differed between 2017  
88 and 2018, and 3) that the hydrography, including sea-ice condition before sampling, will  
89 affect the diatom community.

90

91

## 92 **2. Materials and methods**

93

94 *2.1. Study area*

95

96           Sampling was conducted along the northern Bering Sea shelf from July 9–21,  
97 2017 and July 2–12, 2018 during the 40th and 56th cruises, respectively, of the *T/S*  
98 *Oshoro-Maru* of Hokkaido University (Fig. 1). The study areas were the waters south of  
99 St. Lawrence Island, the Chirikov Basin (from the north of St. Lawrence Island to the  
100 south of Bering Strait), and the Bering Strait.

101

102 *2.2. Sea Ice*

103

104           Data on sea ice concentration (SIC) were obtained from the Advanced  
105 Microwave Scanning Radiometer 2 (AMSR2) to evaluate the extent of the sea ice. These  
106 AMSR2 data were supplied by the Japan Aerospace Exploration Agency via the Arctic  
107 Data archive System (ADS) (<https://ads.nipr.ac.jp/>), through the cooperation of the  
108 National Institute of Polar Research and JAXA. We used the SIC data after calculating a  
109 5-day moving average. Sea-ice covered regions were defined as having a SIC > 20%. In  
110 addition, the TSR was defined as the last date when the SIC was at 20% prior to the  
111 observed annual sea ice minimum across the study region.

112

113 *2.3. Physical Oceanography*

114

115           Conductivity-temperature-depth (CTD) casts were conducted at 40 stations in  
116 2017 and 28 stations in 2018 to obtain vertical profiles of the temperature, salinity, and  
117 chlorophyll *a* fluorescence (see Appendix Fig. 1). We used a CTD (SBE911, Sea-Bird  
118 Electronics, Inc.) calibrated prior to the cruise. The mixed-layer depth was defined as the

119 depth where density was  $0.10 \text{ kg m}^3$  greater than the value at 5 m depth (Danielson et al.,  
120 2011).

121

#### 122 *2.4. Nutrients*

123

124 At 26 of the CTD stations (14 stations in 2017 and 12 stations in 2018), water  
125 samples for nutrient analysis were collected from 4–6 layers every 10 m from the surface  
126 to 5 m above the seafloor using a bucket and Niskin bottles (Fig. 1). The obtained  
127 unfiltered nutrient samples ( $n = 128$ ) in Spitz tubes were frozen on board at  $-80 \text{ }^\circ\text{C}$ . In the  
128 shore-based laboratory, the major nutrients ( $\text{NO}_2\text{-N} + \text{NO}_3\text{-N}$ ,  $\text{NH}_4\text{-N}$ ,  $\text{PO}_4\text{-P}$ , and  $\text{Si}$   
129  $(\text{OH})_4$ ) were measured by colorimetric methods using a QuAatro 2-HR system certified  
130 with standard reference materials for nutrient analysis (KANSO, standard Lot BT, BZ,  
131 Osaka, Japan) in accordance with “The GO-SHIP Repeat Hydrography Manual” (Hydes  
132 et al., 2010).

133

#### 134 *2.5. Phytoplankton*

135

136 Water samples for phytoplankton counts were collected from the same stations  
137 and layers as the nutrient samples. A total of 141 phytoplankton samples was collected  
138 and preserved as follows: in 2017, 500 mL water samples were concentrated 50-fold using  
139 a nucleopore filter ( $3.0 \text{ } \mu\text{m}$ ) before being preserved with glutaraldehyde at a final  
140 concentration of 1%. Note that the diatoms and dinoflagellates addressed in this study  
141 experience little damage from filtering (Dahl and Naustvoll, 2010). In 2018, 1 L of each  
142 water sample was preserved on board with glutaraldehyde at a final concentration of 1%.  
143 The samples were then settled and concentrated 24- to 33- fold using siphon tubes in the

144 land laboratory.

145 Aliquots (1 mL) of the concentrated samples were transferred to a glass slide to  
146 count and identify the diatoms and dinoflagellates with an inverted microscope at 200–  
147 600 × magnification. The diatoms and dinoflagellates were counted and identified from  
148 approximately 300 cells. When the cell number count was less than 300 cells, the  
149 minimum numbers were 18 cells in 2017 and 21 cells in 2018. In addition, the detection  
150 limits were 20 cells L<sup>-1</sup> in 2017 and 30 cells L<sup>-1</sup> in 2018, suggesting that there was not  
151 much difference (ability to detect low numbers of cells in a sample) between the years.  
152 As explained in Hasle and Syvertsen (1997) and Hoppenrath et al. (2009), the diatoms  
153 were identified to the species or genus level and the dinoflagellates were identified to the  
154 genus level. Distinguishing *Cylindrotheca closterium* from *Nitzschia longissima* was  
155 difficult (Hasle and Syvertsen, 1997), so these species were treated as *Cy. closterium*. In  
156 addition, *C. convolutus*, *C. concavicornis* and *C. borealis* were nearly indistinguishable  
157 because they were damaged by current transportation, as mentioned by Taniguchi et al.  
158 (1976), so they were collectively counted and identified as *C.*  
159 *convolutus/concavicornis/borealis*.

160 Using the counting data, the diversity of diatoms was evaluated by Shannon-  
161 Wiener index ( $H'$ ).

$$162 \quad H' = - \sum \frac{n}{Ni} \times \ln \frac{n}{Ni}$$

163 where  $n$  is the cell density (cells mL<sup>-1</sup>) of  $i$ th species and  $Ni$  is the total diatom cell density  
164 (cells mL<sup>-1</sup>) at each station (Shannon and Weaver, 1949).

165

## 166 2.6. Statistical analyses

167

168 Differences in phytoplankton cell density among the water masses in the upper

169 mixed-layer was tested by Mann-Whitney U-test. For comparison of the diatom  
170 community among the water masses, we performed cluster analyses, nonmetric  
171 multidimensional scaling (NMDS) ordinations, and multiple regression analyses for each  
172 year or with each water mass, but the results could not be interpreted (cf. Appendix Figs.  
173 2, 3). Also, to compare the diatom diversity ( $H'$ ) among the water masses, a one-way  
174 analysis of variance (ANOVA) was used. If the ANOVA identified statistically significant  
175 differences ( $p < 0.05$ ), a post hoc Tukey-Kramer test was used to clarify the interactions  
176 among the water masses.

177         Differences between the years of the  $\text{NO}_2\text{-N} + \text{NO}_3\text{-N}$  concentration, which was  
178 likely to be a limiting factor among nutrients, were compared by a Mann-Whitney U-test  
179 for each region. Similarly, differences of the phytoplankton cell density between 2017  
180 and 2018 in the Bering Strait, and of diatom diversity ( $H'$ ) between 2017 and 2018 were  
181 tested using a Mann-Whitney U-test.

182         To compare the diatom community between 2017 and 2018, we first performed  
183 a cluster analysis based on the cell density within each water mass (Appendix Fig. 2).  
184 Several patterns of the cluster analysis were tested in each year, by water mass, and by  
185 depth (cf. Appendix Figs. 2, 3). The results of these tests were uninterpretable, so we used  
186 analyses based on all diatom samples from a given year. Thus, this analysis focused on  
187 describing year-to-year changes in the diatom community (species composition) between  
188 2017 and 2018. To reduce the bias for abundant species, the cell density data ( $X$ : cells  
189  $\text{mL}^{-1}$ ) for each species were transformed to  $\sqrt[4]{X}$  prior to cluster analysis (Quinn and  
190 Keough, 2002). The similarities between samples were examined using the Bray-Curtis  
191 index based on the differences in the species composition. To group the samples, the  
192 similarity indices were coupled using hierarchical agglomerative clustering with a  
193 complete linkage method (an unweighted pair group method using the arithmetic mean)

194 (Field et al., 1982).

195 To delineate the sample groups on a two-dimensional map, NMDS ordination  
196 was conducted. Thereafter, multiple regression analyses ( $Y = aX_1 + bX_2 + c$ , where  $Y$  is  
197 the environmental variable and  $X_1$  and  $X_2$  are axes 1 and 2 of NMDS, respectively) were  
198 performed to clarify which environmental variables (temperature, salinity, chlorophyll  $a$   
199 fluorescence, concentrations of  $\text{NO}_2\text{-N} + \text{NO}_3\text{-N}$ ,  $\text{NH}_4\text{-N}$ , dissolved inorganic nitrogen  
200 (DIN),  $\text{PO}_4\text{-P}$ , and  $\text{Si}(\text{OH})_4$ , the ratio of the DIN concentration to that of  $\text{PO}_4\text{-P}$  (N:P ratio),  
201 the timing of the sea-ice retreat (TSR), observation date, and sampling depth) had  
202 significant relationships with the phytoplankton groups.

203 Furthermore, to test intergroup differences in the diatom cell density and  
204 hydrographic environments (temperature, salinity, chlorophyll  $a$  fluorescence,  
205 concentrations of  $\text{NO}_2\text{-N} + \text{NO}_3\text{-N}$ ,  $\text{NH}_4\text{-N}$ , DIN,  $\text{PO}_4\text{-P}$ , and  $\text{Si}(\text{OH})_4$ , the N:P ratio, and  
206 the TSR), a one-way ANOVA and a post hoc Tukey-Kramer test were used. All the  
207 analyses were conducted with PRIMER 7 (PRIMER-E Ltd.) or Stat View v5 (SAS  
208 Institute Inc.).

209

210

### 211 **3. Results**

212

#### 213 *3.1. Sea Ice*

214

215 In 2017, the study region south of St. Lawrence Is. was first completely ice-  
216 covered on January 19, and in 2018, sea-ice cover was not complete until February 5. The  
217 sea ice first covered the Bering Strait and the Chirikov Basin, except for the most eastern  
218 station, on January 11, 2017 and December 28, 2018. In some stations in 2018 (St. 11 and

219 St. 14), the SIC was repeatedly over and below 20%. In the most eastern stations in the  
220 Chirikov Basin (St. 5 in 2017 and St. 19 in 2018), the SIC exceeded 20% on December  
221 8, 2016 and 2017.

222 South of St Lawrence Island, in 2017, sea ice was completely gone by May 3,  
223 whereas in 2018, ice left over a month earlier, on March 24. In 2017, the first day in the  
224 study area when the Chirikov Basin had an ice concentration  $< 20\%$  was on April 5,  
225 whereas, in 2018, open water was first detected on March 25, 11 days earlier.

226

### 227 *3.2. Hydrography and nutrient chemistry*

228

229 We identified four water masses that differed in physical characteristics; Bering  
230 Chukchi Summer Water (BCSW) (moderate/cold with high salinity), Bering Chukchi  
231 Winter Water (BCWW) (cold with high salinity), Alaskan coastal water (ACW) (warm  
232 with low salinity), and Melting Water (MW) (cold with low salinity) (Danielson et al.,  
233 2017) (Figs. 2, 3). The water masses ( $> 12\text{ }^{\circ}\text{C}$  in ACW and  $> 7\text{ }^{\circ}\text{C}$  in BCSW) that were  
234 unidentified by Danielson et al. (2017) were defined as ACW or BCSW based on their  
235 salinity (Fig. 3).

236 In 2017, the BCWW ( $< 0\text{ }^{\circ}\text{C}$ ) was present at the bottom south of St. Lawrence  
237 Island (Fig. 4). The BCSW was present throughout the water column in the Bering Strait  
238 and the northern Chirikov Basin. By contrast, in the eastern coastal area and south of  
239  $65\text{ }^{\circ}\text{N}$  in the Chirikov Basin, the ACW was present in the surface layer and the BCSW  
240 was observed in the lower layer (Fig. 4).

241 In 2018, the BCWW ( $< 0\text{ }^{\circ}\text{C}$ ) was not present at the bottom in the region South  
242 of St. Lawrence Island (Fig. 4). The BCSW was present throughout the water column in  
243 the Bering Strait and the Chirikov Basin, except for the eastern coastal area where the

244 ACW was observed in the surface layer (Fig. 4).

245 The distribution of water masses differed between the years. In 2017, ACW was  
246 present in the surface layer of the southwestern Chirikov Basin and there was BCSW at  
247 the bottom south of St. Lawrence Island; these were not present in 2018.

248 In both years south of St. Lawrence Island, fluorescence above the pycnocline  
249 (avg = 0.07 and 0.16 in 2017 and 2018, respectively) was lower than that below the  
250 pycnocline (avg = 0.39 and 0.60 in 2017 and 2018, respectively) (Fig. 5). In Bering Strait,  
251 fluorescence was similar in both years (2017, avg = 0.90; 2018, avg = 0.78) (Fig. 5). In  
252 the Chirikov Basin, fluorescence above the pycnocline was higher in 2017 (avg = 0.69)  
253 than in 2018 (avg = 0.26), while, below the pycnocline fluorescence was similar in both  
254 years (Fig. 5).

255 To the south of St. Lawrence Island, the  $\text{NO}_2\text{-N} + \text{NO}_3\text{-N}$  was depleted in the  
256 upper mixed layer in both years, but it was high below the pycnocline (Fig. 5) with no  
257 significant differences between the years (*U-test*,  $p > 0.05$ ). In the Bering Strait,  $\text{NO}_2\text{-N}$   
258 +  $\text{NO}_3\text{-N}$  did not differ significantly between years (*U-test*,  $p > 0.05$ ) (Fig. 5). In this  
259 region, the lowest concentration of nitrate plus nitrite was at the eastern station (st. 5) in  
260 2017, whereas in 2018, the highest concentrations were found in the northern Bering  
261 Strait (st. 29). In the Chirikov Basin, these nutrients were not significantly different  
262 between the years (*U-test*,  $p > 0.05$ ); in both years, the lowest concentrations were  
263 detected at the eastern stations (st. 11 in 2017 and st. 19 in 2018).

264 Concentrations of other nutrients were generally similar between years at the  
265 same station. In both years in each region,  $\text{NH}_4\text{-N}$  concentrations were similar (Fig. 5).  
266 Likewise, the  $\text{PO}_4\text{-P}$  concentrations did not vary between years within regions; the highest  
267 value detected was in the Bering Strait in 2017 (st.1, 6.62  $\mu\text{M}$ ) (Fig. 5). We found high  
268 concentrations of  $\text{Si}(\text{OH})_4$  over major portions of the study region in both years, except

269 for some stations in 2018 in the eastern Chirikov Basin (st. 11 in 2018) and the south of  
270 St. Lawrence Island (sts. 4, 6, 8 in 2018), where this nutrient was not detectable (Fig. 5).  
271 In both years, the N:P ratio was below 16 throughout most of the study area.

272

### 273 3.3. Phytoplankton community

274

#### 275 3.3.1. Cell density

276 In the upper mixed layer, the cell density of diatoms and dinoflagellates was  
277 significantly different in each water mass, and it was higher in BCSW than in ACW  
278 (*Mann-Whitney U-test*,  $p < 0.05$ ), whereas, cell densities below the pycnocline did not  
279 differ among water masses (*one-way ANOVA*,  $p > 0.05$ ). In both 2017 and 2018, the  
280 highest cell densities were observed in the Bering Strait (2017:  $1.6 \times 10^6$  cells L<sup>-1</sup> and in  
281 2018:  $3.4 \times 10^5$  cells L<sup>-1</sup>) with diatoms and dinoflagellates in this region more abundant  
282 in 2017 (stations 1–3) than in 2018 (stations 27–30) (*Mann-Whitney U-test*,  $p < 0.05$ ) (Fig.  
283 6).

284

#### 285 3.3.2. Phytoplankton species and their diversity

286 A total of 29 genera and 30 species of diatoms (centric diatoms: 19 genera and  
287 25 species and pennate diatoms: 10 genera and 5 species) and 6 genera and 5 species of  
288 dinoflagellate were observed over the two years (Table 1).

289 The diversity of the diatoms ( $H'$ ) ranged from 0–3.56 in 2017 and 0.36–2.98 in  
290 2018. The  $H'$  varied among water masses, with values significantly higher in BCWW and  
291 BCSW than in ACW (*one-way ANOVA*,  $p < 0.05$ ). There were no significant differences  
292 in the diversity of diatoms between the years (*Mann-Whitney U-test*,  $p > 0.05$ ).

293

### 294 3.3.3. Phytoplankton community by cluster analysis

295 Phytoplankton communities were classified into four groups (A–D) by a cluster  
296 analysis at 27% and 37% similarity levels (Fig. 7a). Group A was low-density ( $1.3 \times 10^3$ –  
297  $1.3 \times 10^5$  cells L<sup>-1</sup>, avg =  $4.6 \times 10^4$  cells L<sup>-1</sup>) and was composed primarily of *C. gelidus*  
298 (Fig. 7b). Group B had the highest cell density ( $1.6 \times 10^3$ – $1.6 \times 10^6$  cells L<sup>-1</sup>, avg =  $2.5 \times$   
299  $10^5$  cells L<sup>-1</sup>), and *Hyalochaetae* such as *C. gelidus*, *C. furcellatus*, and *C. debilis* were  
300 dominant (64%) (Fig. 7b). The cell density of *C. gelidus*, *C. diadema*, and *Chaetoceros*  
301 spp. in group B was significantly higher than it was in groups C and D. The cell density  
302 of group C was nearly as low as it was in group A ( $3.3 \times 10^3$ – $1.2 \times 10^5$  cells L<sup>-1</sup>, avg =  
303  $3.4 \times 10^4$  cells L<sup>-1</sup>); however, the community composition was very different. *Phaeoceros*  
304 such as *C. convolutus/concavicornis/borealis* had a relatively high density in group C  
305 (13%), and the pennate diatoms such as *Thalassionema nitzschioides* and *Cylindrotheca*  
306 *closterium* had a significantly higher density in group C than it did in the other groups  
307 (Table 2). Group D had the lowest cell density ( $3.6 \times 10^2$ – $4.4 \times 10^5$  cells L<sup>-1</sup>, mean  $2.5 \times$   
308  $10^4$  cells L<sup>-1</sup>) and *Leptocylindrus* spp. dominated (85%).

309 The phytoplankton communities were different in each region (Fig. 7c). In both  
310 years south of St. Lawrence Island, group D was present in the upper layer (0 m or 0–20  
311 m) and groups A, B, and C occurred in the deeper layers. From 65°N (the Chirikov Basin)  
312 to the Bering Strait, the distribution varied across years; group B was observed throughout  
313 the area in 2017, but group C was observed in 2018. In these regions (the Chirikov Basin  
314 and the Bering Strait), the spatial distribution of water masses and phytoplankton  
315 community groups as determined by the cluster analysis did not match (Fig.4, Fig.7c),  
316 thus, the groups were different between years even though BCSW was occupied in both  
317 years.

318

### 319 3.3.4. Relationships between phytoplankton communities and environmental factors

320 On the NMDS ordination, phytoplankton plots had significant relationships with  
321 various environmental variables ( $p < 0.05$ ), including chlorophyll *a* fluorescence ( $r^2 =$   
322 0.30), TSR ( $r^2 = 0.28$ ), observation date ( $r^2 = 0.16$ ), sampling depth ( $r^2 = 0.13$ ), salinity  
323 ( $r^2 = 0.11$ ), Si (OH)<sub>4</sub> ( $r^2 = 0.08$ ) and NO<sub>2</sub>+NO<sub>3</sub> ( $r^2 = 0.05$ ) (Fig. 7d), but the other  
324 parameters did not. Especially note that temperature did not have a significant relationship  
325 with phytoplankton plots ( $p > 0.05$ ), and that the contribution of TSR to diatom groups  
326 was the highest among environmental factors except for chlorophyll *a* fluorescence.

327 In addition, the one-way ANOVA and Tukey-Kramer test indicated that the PO<sub>4</sub>  
328 and DIN concentrations and the N:P ratio did not differ significantly among  
329 phytoplankton groups (*one-way ANOVA*,  $p > 0.05$ ). However, the other hydrographic  
330 variables differed between groups B and D. Group D had a higher temperature and lower  
331 salinity, nutrients (NO<sub>2</sub>+NO<sub>3</sub>, PO<sub>4</sub>-P, NH<sub>4</sub>-N, Si (OH)<sub>4</sub>), and chlorophyll *a* fluorescence  
332 than the other groups. Groups B and C differed only in their salinity, chlorophyll *a*  
333 fluorescence and TSR (Table 3). Especially note that temperature was not significantly  
334 different between Group B and C.

335

336

## 337 4. Discussion

338

### 339 4.1. The influence of water masses

340

341 Diatom community structure (i.e. species composition and their cell density) was  
342 not consistently correlated with water mass during summer except for the stations south  
343 of St. Lawrence Island. However, there were significant differences among the water

344 masses in the cell density in the upper mixed layer and in diatom diversity. These  
345 differences may have been related to differences in the nutrient content of the water  
346 masses. Differences in characteristics of water masses are known to influence  
347 phytoplankton cell density (Coachman et al., 1975; Danielson et al., 2017; Giesbrecht et  
348 al., 2019). The N:P ratio was below 16 throughout the study area, which indicated that  
349 the DIN was the limiting nutrient concentration, and differences in DIN concentrations in  
350 the various water masses was one of the most important factors for the growth of  
351 phytoplankton upper the mixed layer over the study area. Thus, phytoplankton cell  
352 density was higher in the upper mixed layer in the BCSW, including the nutrient-rich AW,  
353 than in the nutrient-poor ACW (Coachman et al., 1975; Danielson et al., 2017).

354         The diversity of diatoms indicated by  $H'$  was higher in BCWW and BCSW than  
355 in ACW in the same way as the DIN concentration was. We suggest that the differences  
356 in the diversity of diatoms between water masses was related to difference in nutrient  
357 concentrations between water masses, especially the DIN concentrations. As mentioned  
358 above, DIN was the limiting factor in the nutrient concentration and thus, in the water  
359 masses with high DIN such as BCWW and BCSW, competition for DIN may have been  
360 minimal, thus resulting in many diatom species surviving in these waters.

361

#### 362 *4.2. The phytoplankton community of the south of St. Lawrence Island*

363

364         In contrast to the Chirikov Basin and the Bering Strait regions, south of St  
365 Lawrence Island year-to-year changes in the phytoplankton community were not  
366 observed. In the upper mixed layer south of St. Lawrence Island, nutrient-poor ACW was  
367 present in both years, and the DIN concentrations and, at some stations the  $\text{Si (OH)}_4$   
368 concentrations, were too low to support diatom growth (Justic et al., 1995). The lack of

369 DIN may have resulted in the dominance of phytoplankton group D, which was  
370 predominately non-diatom species that can thrive in low nutrient conditions (Parsons et  
371 al., 1978). The timing and magnitude of the spring phytoplankton bloom in the region  
372 south of St. Lawrence Island differed in 2017 and 2018, and we hypothesize that this was  
373 due to differences in the TSR (Fukai et al., 2019; Hirawake, per. comm.). Thus, after the  
374 nutrients were depleted from the upper mixed layer, phytoplankton, other than diatoms,  
375 dominated. A similar succession may occur in the eastern Bering Sea where  
376 coccolithophore blooms during the summer were reported after the diatom bloom  
377 (Stockwell et al., 2001; Iida et al., 2002). Coccolithophore blooms were also observed by  
378 satellite observation from the eastern Bering Sea to south of St. Lawrence Island after  
379 2000s (Harada et al., 2012). In our study, it is not clear whether the phytoplankton  
380 community changed at the species level, because dinoflagellates and phytoplankton other  
381 than diatoms were not identified to the species level.

382

#### 383 *4.3. The changes in the summer diatom community in the Chirikov Basin and the Bering* 384 *Strait, 2017-2018*

385

386 From 65°N (the Chirikov Basin) to the Bering Strait, between 2017 and 2018,  
387 phytoplankton cell density declined and community structure changed. In this region in  
388 2017, the highest cell density ( $1.6 \times 10^6$  cells L<sup>-1</sup>) was nearly the same as that reported by  
389 Sergeeva et al. (2010) for July 2003 and by Giesbrecht et al. (2019) (the highest density  
390 was approximately  $10^6$  cells L<sup>-1</sup>). In 2018, the highest cell density ( $3.4 \times 10^5$  cells L<sup>-1</sup>)  
391 was only 34% of the values observed in 2017.

392 With respect to the phytoplankton community, in 2017, group B was widely  
393 distributed and had a high cell density that was dominated (64%) by *Hyalochaetae* such

394 as *C. gelidus* and *C. furcellatus*. *C. gelidus* and *C. furcellatus* are cold-water species and  
395 are common in the Arctic (Hasle and Syvertsen, 1997; Hoppenrath, 2009). These species  
396 are typically found in the Chukchi Sea adjacent to the study area (von Quillfeldt et al.,  
397 2003). In 2018, Group C, which was mostly composed of *Thalassionema nitzschioides*,  
398 was widely distributed. The abundance of *Chaetoceros* spp. was low (20%), and  
399 *Phaeoceros* such as *C. convolutus/concavicornis/borealis* made up most of the  
400 *Chaetoceros* spp. *T. nitzschioides* and *C. convolutus* are known as cosmopolitan species;  
401 the former does not occur in the high Arctic and the latter is common in temperate waters  
402 (Hasle and Syvertsen, 1997; Hoppenrath, 2009). *T. nitzschioides* has also been reported  
403 in temperate water after the melting of the sea ice (Neeley et al., 2018), and it is a  
404 characteristic species of the Pacific-Arctic region in the autumn (Matsuno et al., 2014).  
405 These results suggest that between 2017 and 2018, the summer diatom community in the  
406 Bering Strait and the Chirikov Basin changed from cold water to cosmopolitan species.

407         Interestingly, the NMDS, the multiple regressions, and the one-way ANOVA did  
408 not suggest any significant differences in temperature between 2017 and 2018 in the  
409 region north of 65°N. By contrast, the TSR was the most important contributing factor  
410 among the environmental factors for explaining the differences in the diatom  
411 communities between the two years. There was also a significant difference in the TSR  
412 between group B in 2017 and C in 2018. Because the TSR differed between 2017 and  
413 2018 in the northern Bering Sea (Cornwall, 2019; Fukai et al., 2019; Grebmeier et al.,  
414 2019), the effect of the TSR on the summer diatom community cannot be ignored.

415         The TSR affects the magnitude and timing of the spring bloom in the seasonal  
416 sea ice area (Hunt et al., 2002; Fujiwara et al., 2016). The magnitude of the phytoplankton  
417 bloom in the open water is usually large when the TSR is early (Hunt et al., 2002; Fujiwara  
418 et al., 2016). In 2018, when the TSR was early, large increases in sea surface chlorophyll

419 *a* in the Chirikov Basin were observed with satellite remote sensing from early to late  
420 May after the sea ice had completely retreated (Hirawake, per. comm.). Hence, in 2018,  
421 when the TSR was early, the available nutrients may have been consumed by the large  
422 open-water bloom during early spring after the sea ice retreat, resulting in the wide  
423 distribution of phytoplankton community group C during summer, with a low cell density.  
424 In summer 2018, the cosmopolitan species composition of group C, some of which, such  
425 as *T. nitzschioides*, are species characteristic of the autumn (Matsuno et al., 2014), and  
426 might been the result of the early TSR in 2018 and an early depletion of nutrients.

427

428

## 429 **5. Conclusions**

430

431 This study described and compared northern Bering Sea diatom communities in  
432 the summers of 2017 and 2018. The diatom cell density and diatom diversity differed by  
433 water mass. Year-to-year differences in the diatom community between 2017 and 2018  
434 were found, depending on the region examined. South of St. Lawrence Island, we found  
435 no changes in the diatom community between 2017 and 2018. Nitrate and nitrite were  
436 depleted in the upper mixed layer in both years, and phytoplankton types other than  
437 diatoms dominated this region. Since we focused our study on diatoms, it is possible that  
438 there were interannual changes in other elements of the phytoplankton community that  
439 we did not detect.

440 In the Chirikov Basin and Bering Strait, diatom communities in 2017 and 2018  
441 differed, even though the same water masses were present in both years. The TSR was  
442 much earlier in 2018 than in 2017, though summer water temperatures were similar in the  
443 two years. Since nutrient concentrations were lower in 2018, we hypothesize that the open

444 water bloom in 2018 may have depleted the nutrients, with the result that in 2018 several  
445 sub-arctic or cosmopolitan species were abundant compared to 2017, when arctic species  
446 predominated. It will be important to evaluate the influence of the changing diatom  
447 community on the marine ecosystem of the northern Bering and Chukchi Seas. To this  
448 end, focus on the entire phytoplankton community, including dinoflagellates,  
449 coccolithophores and others, will be required.

450

451

## 452 **Acknowledgments**

453

454 We thank the captain, officers, crew, and researchers on board the *T/S Oshoro-*  
455 *Maru*, of Hokkaido University, for their contributions during field sampling. We thank  
456 Toru Hirawake, chief scientist of the cruises. We also thank two anonymous reviewers for  
457 their helpful comments. This study was conducted by the Arctic Challenge for  
458 Sustainability (ArCS) project and Arctic Challenge for Sustainability II (ArCS II) project.  
459 The ADS dataset is archived and was provided by the Arctic Data archive System (ADS),  
460 which was developed by the National Institute of Polar Research. Part of this study was  
461 supported through Grants-in-Aid for Scientific Research 17H01483 (A), 19H03037 (B),  
462 20H03054 (B), 18K14506 (Early-Career Scientists) and 20K20573 (Challenging  
463 Research (Pioneering)) from the Japan Society for the Promotion of Science.

464

465 **References**

466

467 Coachman, L.K., Aagaard, K., Tripp, R.B., 1975. Bering Strait: The regional physical  
468 oceanography. University of Washington Press, Seattle, WA.

469 Cornwall, W., 2019. Vanishing Bering Sea ice poses climate puzzle for second winter in  
470 a row, ice cover shrinks to lowest levels seen in at least 4 decades. *Science*  
471 364, 616–617.

472 Dahl, E., Naustvoll, L.J., 2010. Filtering – semitransparent filters for quantitative  
473 phytoplankton analysis. In: Karlson, B., Cusack, C., Bresnan, E. (Eds.).  
474 Microscopic and molecular methods for quantitative phytoplankton analysis.  
475 UNESCO, Paris, 37–39.

476 Danielson, S., Eisner, L., Weingartner, T., Aagaard, K., 2011. Thermal and haline  
477 variability over the central Bering Sea shelf: Seasonal and interannual  
478 perspectives. *Cont. Shelf Res.*, 31, 539–554.

479 Danielson, S.L., Eisner, L., Ladd, C., Mordy, C., Sousa, L., Weingartner, T.J., 2017. A  
480 comparison between late summer 2012 and 2013 water mass, macronutrients,  
481 and phytoplankton standing crops in the northern Bering and Chukchi. *Deep-*  
482 *Sea Res. II*, 135, 7–26.

483 Duffy-Anderson, J.T., Stabeno, P., Andrews III, A.G, Ciciel, K., Deary, A., Farley, E.,  
484 Fugate, C., Harpold, C., Heintz, R., Kimmel, D., Kuletz, K., Lamb, J., Paquin,  
485 M., Porter, S., Rogers, L., Spear, A., Yasumiishi, E., 2019. Responses of the  
486 Northern Bering Sea and southeastern Bering Sea pelagic ecosystems  
487 following record-breaking low winter sea ice. *Geophys. Res. Let.* 46, 9833–  
488 9842.

489 Field, J.G., Clarke, K.R., Warwick, R.M., 1982. A practical strategy for analyzing

490 multispecies distribution patterns. *Mar. Ecol. Prog. Ser.* 8, 37–52.

491 Frey, K.E., Comiso, J.C., Cooper, L.W., Grebmeier, J.M., Stock, L.V., 2018. Arctic ocean  
492 primary productivity: the response of marine algae to climate warming and  
493 sea ice decline. In: *Arctic Report Card. Arctic Region 2018*,  
494 <http://www.arctic.noaa.gov/reportcard>).

495 Fujiwara, A., Hirawake, T., Suzuki, K., Eisner, L., Imai, I., Nishino, S., Kikuchi, T., Saitoh,  
496 S.-I., 2016. Influence of timing of sea ice retreat on phytoplankton size  
497 during marginal ice zone bloom period on the Chukchi and Bering shelves.  
498 *Biogeosciences* 13, 115–131.

499 Fukai, Y., Matsuno, K., Fujiwara, A., Yamaguchi, A., 2019. The community composition  
500 of diatom resting stages in sediments of the northern Bering Sea in 2017  
501 and 2018: the relationship to the interannual changes in the extent of the sea  
502 ice. *Polar Biol.* 42, 1915–1922.

503 Giesbrecht, K.E., D.E. Varela, J. Wiktor, J.M. Grebmeier, B. Kelly, J.E. Long, 2019. A  
504 decade of summertime measurements of phytoplankton biomass,  
505 productivity and assemblage composition in the Pacific Arctic Region from  
506 2006 to 2016. *Deep-Sea Res. II* 162, 93–113.

507 Grebmeier, J.M., McRoy, C.P., Feder, H.M., 1988. Pelagic-benthic coupling on the shelf  
508 of the northern Bering and Chukchi Seas. I. Food supply source and benthic  
509 biomass. *Mar. Ecol. Prog. Ser.* 48, 57–67.

510 Grebmeier, J.M., Bluhm, B.A., Cooper, L.W., Danielson, S.L., Arrigo, K.R., Blanchard,  
511 A.L., Clarke, J.T., Day, R.H., Frey, K.E., Gradiner, R.R., Kędra, M., Konar,  
512 B., Kuletz, K.J., Lee, S.H., Lovvorn, J.R., Norcross, B.L., Okkonen, S.R.,  
513 2015. Ecosystem characteristics and processes facilitating persistent  
514 macrobenthic biomass hotspots and associated benthivory in the Pacific

515 Arctic. Prog. Oceanogr. 136, 92–114.

516 Grebmeier, J.M., Moore, S.E., Cooper, L.W., Frey, K.E., 2019. The Distributed Biological  
517 Observatory: A change detection array in the Pacific Arctic – An introduction.  
518 Deep-Sea Res. II 162, 1–7.

519 Harada, N., Sato, M., Oguri, K., Hagino, K., Okazaki, Y., Katsuki, K., Tsuji, Y., Shin, K.-  
520 H., Tadaï, O., Saitoh, S.-I., Narita, H., Konno, S., Jordan, R.W., Shiraiwa, Y.,  
521 Grebmeier, J., 2012. Enhancement of coccolithophorid blooms in the Bering  
522 Sea by recent environmental changes. Global Biogeochem. Cycles 26,  
523 GB2036.

524 Hasle, G.R., Syvertsen, E.E., 1997. Marine diatoms. In: Tomas, C.R. (Ed). Identifying  
525 marine phytoplankton. Academic Press, San Diego, 5–385

526 Hoppenrath, M., Elbrächter, M., Drebes, G., 2009. Marine phytoplankton: selected  
527 microphytoplankton species from the North Sea around Helgoland and Sylt.,  
528 Schweizerbart Science Publishers.

529 Hunt, G.L., Stabeno, P., Walters, G., Sinclair, E., Brodeur, R.D., Napp, J.M., Bond, N.A.,  
530 2002. Climate change and control of the southeastern Bering Sea pelagic  
531 ecosystem. Deep-Sea Res. II 49, 5821–5853.

532 Huntington, H.P., Danielson, S.L., Wiese, F.K., Baker, M.R., Boveng, P., Citta, J.J., De  
533 Robertis, A., Dickson, D.M.S., Farley, E.V., George, J.C., Iken, K., Kimmel,  
534 D.G., Kuletz, K., Ladd, C., Levine, R., Quakenbush, L., Stabeno, P., Stafford,  
535 K.M., Stockwell, D., Wilson C., 2020. Evidence suggests potential  
536 transformation of the Pacific Arctic ecosystem is underway. Nat. Clim.  
537 Change 10, 342–349.

538 Hydes, D.J., Aoyama, M., Aminot, A., Bakker, K., Becker, S., Coverly, S., Daniel, A.,  
539 Dickson, A.G., Grosso, O., Kerouel, R., van Ooijen, J., Sato, K., Tanhua, T.,

- 540 Woodward, E.M.S., Zhang, J.Z., 2010. Determination of dissolved nutrients  
541 (N, P, Si) in seawater with high precision and inter-comparability using gas-  
542 segmented continuous flow analysers. In: Hood, E.M., Sabine, C.L., Sloyan,  
543 B.M. (Eds.). The GO-SHIP Repeat Hydrography Manual: A Collection of  
544 Expert Reports and Guidelines. IOCCP report number 14, ICPO publication  
545 series number 134, U.N. Educ. Sci. and Cult. Organ. Intergov. Oceanotr.  
546 Comm., Paris, 1–88.
- 547 Iida, T., Saitoh, S.I., Miyamura, T., Toratani, M., Fukushima, H., Shiga, N., 2002.  
548 Temporal and spatial variability of coccolithophore blooms in the eastern  
549 Bering Sea, 1998-2001. *Prog. Oceanogr.* 55, 165–175.
- 550 Justic, D., Rabalais, N.N., Turner R.E., Dortch, Q., 1995. Changes in nutrient structure of  
551 river-dominated coastal waters: Stoichiometric nutrient balance and its  
552 consequences. *Estuar. Coast. Shelf Sci.* 40, 339–356.
- 553 Matsuno, K., Ichinomiya, M., Yamaguchi, A., Imai, I., Kikuchi, T., 2014. Horizontal  
554 distribution of microprotist community structure in the western Arctic Ocean  
555 during late summer and early fall of 2010. *Polar Biol.* 37, 1185–1195.
- 556 Neeley, A.R., Harris, L.A., Frey, K.E., 2018. Unraveling phytoplankton community  
557 dynamics in the northern Chukchi Sea under sea-ice-covered and sea-ice-  
558 free conditions. *Geophys Res. Lett.* 45, 7663–7671.
- 559 Parsons, T.R., Harrison, P.J., Waters, R., 1978. An experimental simulation of changes in  
560 diatom and flagellate blooms. *J. Exp. Biol. Ecol.* 32, 285–294.
- 561 Quinn, G.P., Keough, M.J., 2002. *Experimental Design and Data Analysis for Biologists.*  
562 Cambridge University Press, New York.
- 563 Sergeeva, V.M., Sukhanova, I.N., Flint, M.V., Pautova, L.A., Grebmeier, J.M., Cooper,  
564 L.W., 2010. Phytoplankton community in the western Arctic in July–August

565                   2003. *Oceanology* 50, 184–197.

566 Shannon, C.E., Weaver, W., 1949. *The mathematical theory of communication*. The  
567                   University of Illinois Press, Urbana.

568 Springer, A.M., McRoy, C.P., 1993. The paradox of pelagic food webs in the northern  
569                   Bering Sea III. Patterns of primary production. *Cont. Shelf. Res.* 13, 575–  
570                   599.

571 Springer, A.M., McRoy, C.P., Flint, M.V., 1996. The Bering Sea Green Belt: shelf-edge  
572                   processes and ecosystem production. *Fish. Oceanogr.* 5(3/4), 205–223.

573 Stockwell, D.A., Whitley, T.E., Zeeman, S.I., Coyle, K.O., Napp, J.M., Brodeur, R.D.,  
574                   Pinckuk, A.I., Hunt, G.L. 2001. Anomalous conditions in the south-eastern  
575                   Bering Sea, 1997: nutrients, phytoplankton and zooplankton. *Fish. Oceanogr.*  
576                   10, 99–116.

577 Taniguchi, A., Saito, K., Koyama, A., Fukuchi, M., 1976. Phytoplankton communities in  
578                   the Bering Sea and adjacent seas I. Communities in early warming season in  
579                   southern areas. *J. Oceanogr. Soc. Jpn.* 32, 99–106.

580 von Quillfeldt, C.H., 2000. Common diatom species in Arctic spring blooms: Their  
581                   distribution and abundance. *Bot. Mar.* 43, 499–516.

582 von Quillfeldt, C.H., Ambrose Jr., W.G., Clough, L.M., 2003. High number of diatom  
583                   species in first-year ice from the Chukchi Sea. *Polar Biol.* 26, 806–818.

584

585 **Figure legends**

586 **Fig. 1.** Location of stations in the northern Bering Sea from July 9–21, 2017 and  
587 July 2–12, 2018. The numbers indicate the station ID. The open and solid  
588 circles indicate stations with hydrographic observations only taken by CTD  
589 and those with water sampling and hydrographic observations, respectively.

590 **Fig. 2.** Cross-sectional distributions of the temperature, salinity, and fluorescence in  
591 the northern Bering Sea in 2017 (upper) and 2018 (lower).

592 **Fig. 3.** T-S diagrams of all the stations in 2017 (upper) and 2018 (lower). Note that  
593 the symbols of the stations vary with the geographical location.

594 **Fig. 4.** Spatial distribution of water masses as defined by Danielson et al. (2017).  
595 BCSW: Bering-Chukchi Summer Water, ACW: Alaskan Coastal Water, MW:  
596 Melting Water, and BCWW: Bering-Chukchi Winter Water.

597 **Fig. 5.** Cross-sectional distributions of nutrient ( $\text{NO}_2\text{-N} + \text{NO}_3\text{-N}$ ,  $\text{NH}_4\text{-N}$ ,  $\text{PO}_4\text{-P}$ ,  
598 and  $\text{Si}(\text{OH})_4$ ) concentrations in the northern Bering Sea in 2017 (upper) and  
599 2018 (lower).

600 **Fig. 6.** Horizontal distribution of the average phytoplankton cell density in 2017  
601 (left) and 2018 (right). The circles indicate the mean cell density in the water  
602 column.

603 **Fig. 7.** (a) Results of the cluster analysis based on the phytoplankton cell density  
604 found by Bray-Curtis similarity. (b) Species composition and cell density of  
605 each group. (c) Spatial distribution of the phytoplankton community in the  
606 northern Bering Sea during the summers of 2017 (left) and 2018 (right). (d)  
607 Nonmetric multidimensional scaling plots of the four groups, with *arrows*  
608 and *percentages* indicating the directions of the environmental parameters

609 and the coefficient of determination ( $r^2$ ), respectively. *Obs. date*: observation  
610 date, *Si*: silicate, *Sal*: salinity, *N*: nitrate and nitrite, *TSR*: the timing of sea ice  
611 retreat, *Fluor*: fluorescence, and *Dep*: sampling depth.

612

613 **Appendix Fig 1.** Relationship between the chlorophyll *a* concentration and the  
614 fluorescence.

615 **Appendix Fig 2.** Spatial distribution of the phytoplankton communities in each water  
616 mass (the BCSW (a) and the ACW (b)) by cluster analyses. The cluster  
617 analyses were conducted in each water mass independently. White boxes  
618 indicated water masses that were not the focus of this analysis. Color codes  
619 for the communities were shown different groups analyzed by the cluster  
620 analysis.

621 **Appendix Fig 3.** Spatial distribution of the phytoplankton communities in each year.  
622 Cluster analyses were conducted in each year independently. Color codes for  
623 the communities were shown different groups analyzed by the cluster  
624 analysis.

625

626 Table 1. List of phytoplankton species identified in the water samples that were collected  
 627 from the northern Bering Sea and Bering Strait in July 2017 and 2018.

---

<b>Class Bacillariophyceae</b>		
Order Centrales		
<i>Actinocyclus</i> spp.	<i>C. furcellatus</i>	<i>Ditylum</i> spp.
<i>Actinoptychus</i> spp.	<i>C. gelidus</i>	<i>Eucampia</i> spp.
<i>Attheya</i> spp.	<i>C. lacinosus</i>	<i>Lauderia annulata</i>
<i>Bacterosira bathyomphala</i>	<i>C. lorenzianus</i>	<i>Leptocylindrus danicus</i>
<i>Chaetoceros conturtus</i>	<i>C. mitra</i>	<i>L. minimus</i>
<i>C. convolutus/concavicornis/borealis</i>	<i>C. subtilis</i>	<i>Odontella aurita</i>
<i>C. curvicetus</i>	<i>C. teres</i>	<i>Paralia sulcata</i>
<i>C. danicus</i>	<i>Chaetoceros</i> spp.	<i>Rhizosolenia</i> spp.
<i>C. debilis</i>	<i>Corethron hystrix</i>	<i>Skeletonema</i> spp.
<i>C. decipiens</i>	<i>Coscinodiscus</i> spp.	<i>Stephanopyxis turris</i>
<i>C. diadema</i>	<i>Detonula pumula</i>	<i>Thalassiosira</i> spp.
<i>C. didymus</i>	<i>Dactyliosolen fragilissimus</i>	Other centric diatoms
Order Pennales		
<i>Asteroplanus karianus</i>	<i>Pauelia taeniata</i>	<i>Navicula</i> spp.
<i>Asterionellopsis glacialis</i>	<i>Pleurosigma</i> spp.	<i>Nitzschia</i> spp.
<i>Cylindrotheca closterium</i>	<i>Pseudo-nitzschia</i> spp.	Other pennate diatoms
<i>Thalassionema nitzschioides</i>	<i>Fragilariopsis</i> spp.	
<b>Class Dinophyceae</b>		
<i>Alexandrium</i> spp.	<i>Protoperidinium</i> spp.	<i>Dinophysis norvegica</i>
<i>Ceratium</i> spp.	<i>Heterocapsa triquetra</i>	<i>Dinophysis rudgei</i>
<i>Prorocentrum triestinum</i>	<i>Dinophysis acuta</i>	Other dinoflagellates

---

628

629

630 Table 2. Comparison of phytoplankton species in the phytoplankton community groups  
 631 (A–D). The values are given as the mean cell density ( $\times 10^3$  cells L<sup>-1</sup>) and standard  
 632 deviation in each group. The numbers in parentheses indicate the number of stations. The  
 633 differences among the phytoplankton communities were evaluated by a one-way ANOVA  
 634 and a Tukey-Kramer test. Any groups not connected by the underlines are significantly  
 635 different (\*:  $p < 0.05$ , \*\*:  $p < 0.01$ , and \*\*\*:  $p < 0.005$ ).

636

Species	Group name				One-way ANOVA	Tukey-Kramer test
	A (5)	B (74)	C (41)	D (21)		
<i>C. convolutus/concavicornis/borealis</i>	4.49 ± 6.47	3.56 ± 7.79	4.37 ± 9.50	0.26 ± 1.01	NS	
<i>C. debilis</i>	—	16.45 ± 42.68	0.20 ± 1.05	—	*	Not detected
<i>C. diadema</i>	0.65 ± 1.29	3.35 ± 4.73	0.06 ± 0.20	0.01 ± 0.02	***	<u>D C A B</u>
<i>C. furcellatus</i>	—	49.95 ± 118.66	—	—	**	Not detected
<i>C. gelidus</i>	31.28 ± 44.80	65.46 ± 114.33	0.02 ± 0.06	0.12 ± 0.33	***	<u>C D A B</u>
<i>Chaetoceros</i> spp.	2.22 ± 2.81	13.94 ± 20.48	0.84 ± 2.91	0.50 ± 1.36	***	<u>D C A B</u>
<i>Leptocylindrus danicus</i>	—	15.43 ± 30.69	3.08 ± 10.43	21.01 ± 89.63	NS	
<i>Cylindrotheca closterium</i>	0.05 ± 0.05	1.09 ± 1.03	1.79 ± 1.60	0.15 ± 0.27	***	<u>A D B C</u>
<i>Thalassionema nitzschioides</i>	0.21 ± 0.28	0.68 ± 1.05	7.51 ± 15.35	0.47 ± 0.95	***	<u>A D B C</u>
<i>Pseudo-nitzschia</i> spp.	—	5.23 ± 12.90	1.45 ± 4.94	0.08 ± 0.34	NS	
<i>Fragilariopsis</i> spp.	0.02 ± 0.04	2.92 ± 10.65	0.41 ± 1.09	0.05 ± 0.21	NS	

637

638 Table 3. Hydrographic environmental factors among the phytoplankton communities (A–  
639 D). The values are given as the average and standard deviation of each factor. The  
640 numbers in parentheses indicate the number of stations. The differences among the  
641 phytoplankton communities were evaluated by a one-way ANOVA and a Tukey-Kramer  
642 test. Any groups not connected by the underlines are significantly different (\*:  $p < 0.05$ ,  
643 \*\*:  $p < 0.01$ , and \*\*\*:  $p < 0.005$ ).

Factors	Group name				One-way ANOVA	Tukey-Kramer test
	A (5)	B (74)	C (41)	D (21)		
Temperature	1.97 ± 3.29	3.56 ± 1.66	2.89 ± 2.49	6.21 ± 2.78	**	<u>A C B D</u>
Fluorescence	0.54 ± 0.56	0.75 ± 0.53	0.44 ± 0.17	0.20 ± 0.13	***	<u>D C A B</u>
Salinity	32.00 ± 0.32	32.49 ± 0.41	32.10 ± 0.87	31.58 ± 0.36	***	<u>D A C B</u>
NO <sub>2</sub> +NO <sub>3</sub>	5.68 ± 6.55	9.34 ± 6.38	7.88 ± 6.29	0.96 ± 1.01	**	<u>D A C B</u>
PO <sub>4</sub> -P	1.18 ± 0.65	1.35 ± 0.83	1.42 ± 0.39	0.80 ± 0.32	NS	
NH <sub>4</sub> -N	1.11 ± 1.43	0.78 ± 0.48	0.84 ± 0.61	0.18 ± 0.13	*	<u>D B C A</u>
Si (OH) <sub>4</sub>	29.48 ± 40.68	25.01 ± 13.25	19.10 ± 12.29	8.60 ± 7.69	*	<u>D C B A</u>
DIN	6.79 ± 7.95	10.41 ± 6.76	10.59 ± 13.33	1.13 ± 1.11	NS	
N/P	4.30 ± 3.34	7.24 ± 3.46	6.94 ± 9.78	1.28 ± 1.02	NS	
TSR	91.00 ± 8.22	115.28 ± 14.44	107.78 ± 11.67	99.38 ± 15.44	***	<u>A D C B</u>

644

645

646

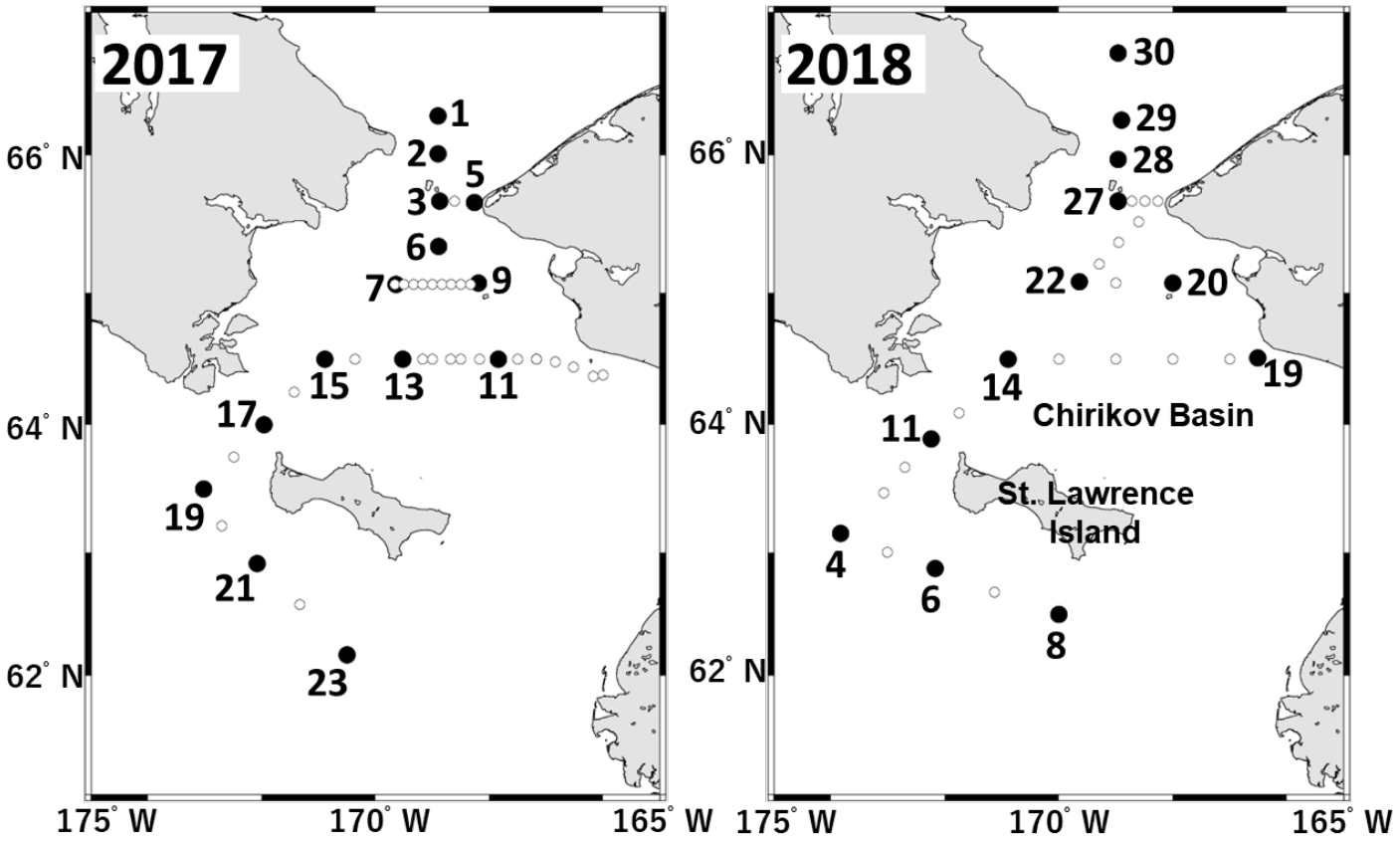


Fig. 1. Location of stations in the northern Bering Sea from July 9–21, 2017 and July 2–12, 2018. The numbers indicate the station ID. The open and solid circles indicate stations with hydrographic observations only taken by CTD and those with water sampling and hydrographic observations, respectively.

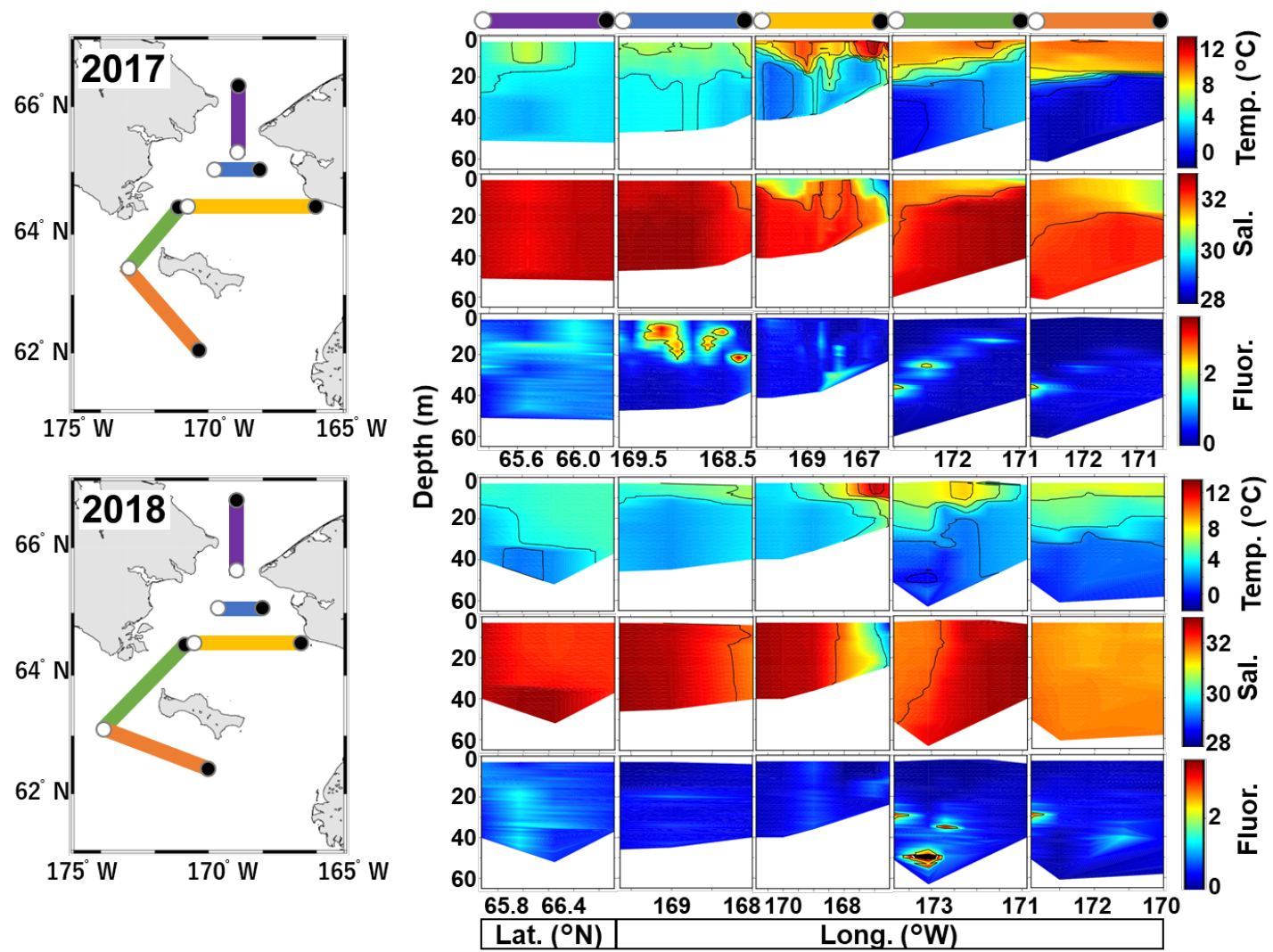


Fig. 2. Cross-sectional distributions of the temperature, salinity, and fluorescence in the northern Bering Sea in 2017 (upper) and 2018 (lower).

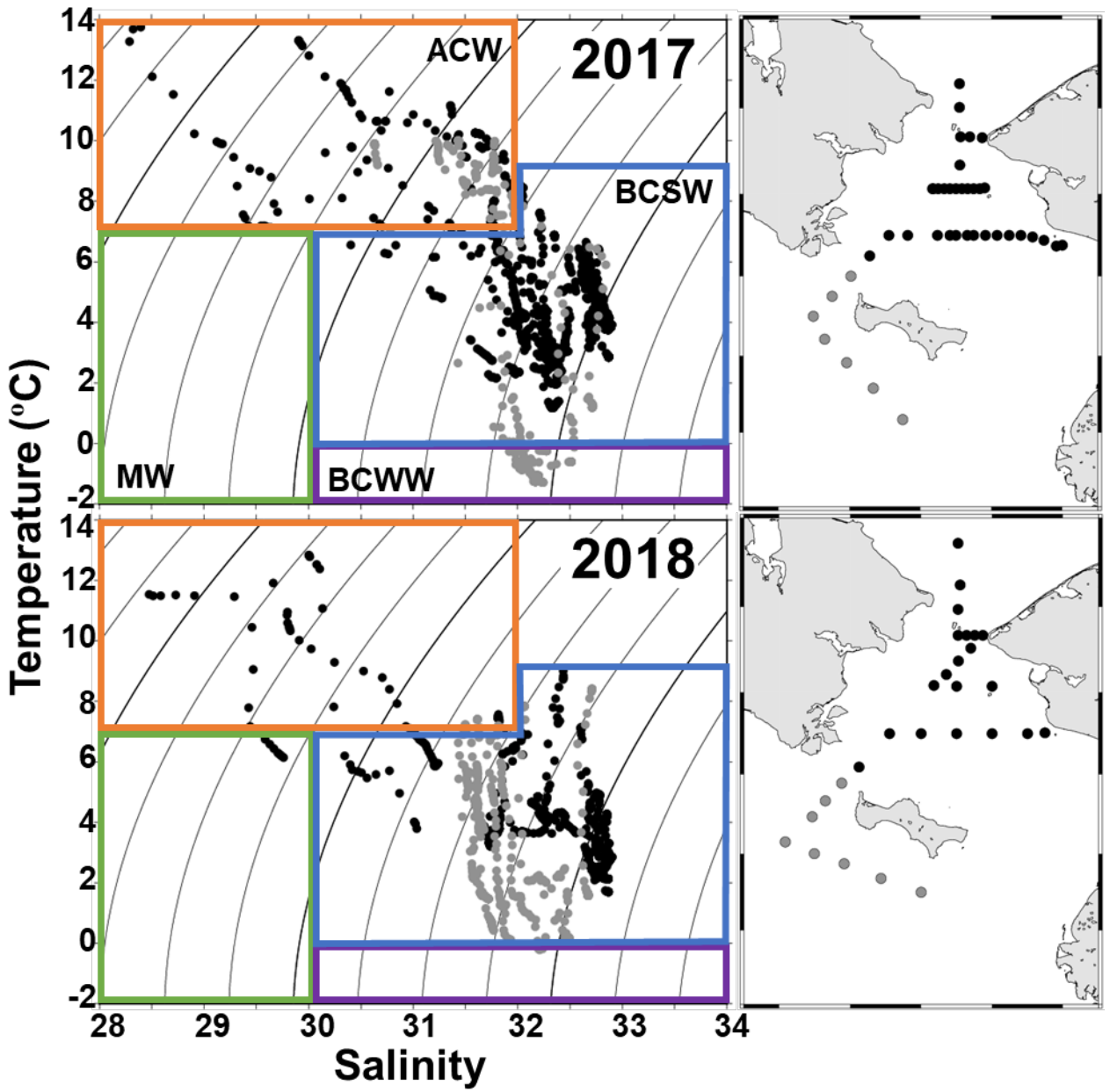


Fig. 3. T-S diagrams of all the stations in 2017 (upper) and 2018 (lower). Note that the symbols of the stations vary with the geographical location.

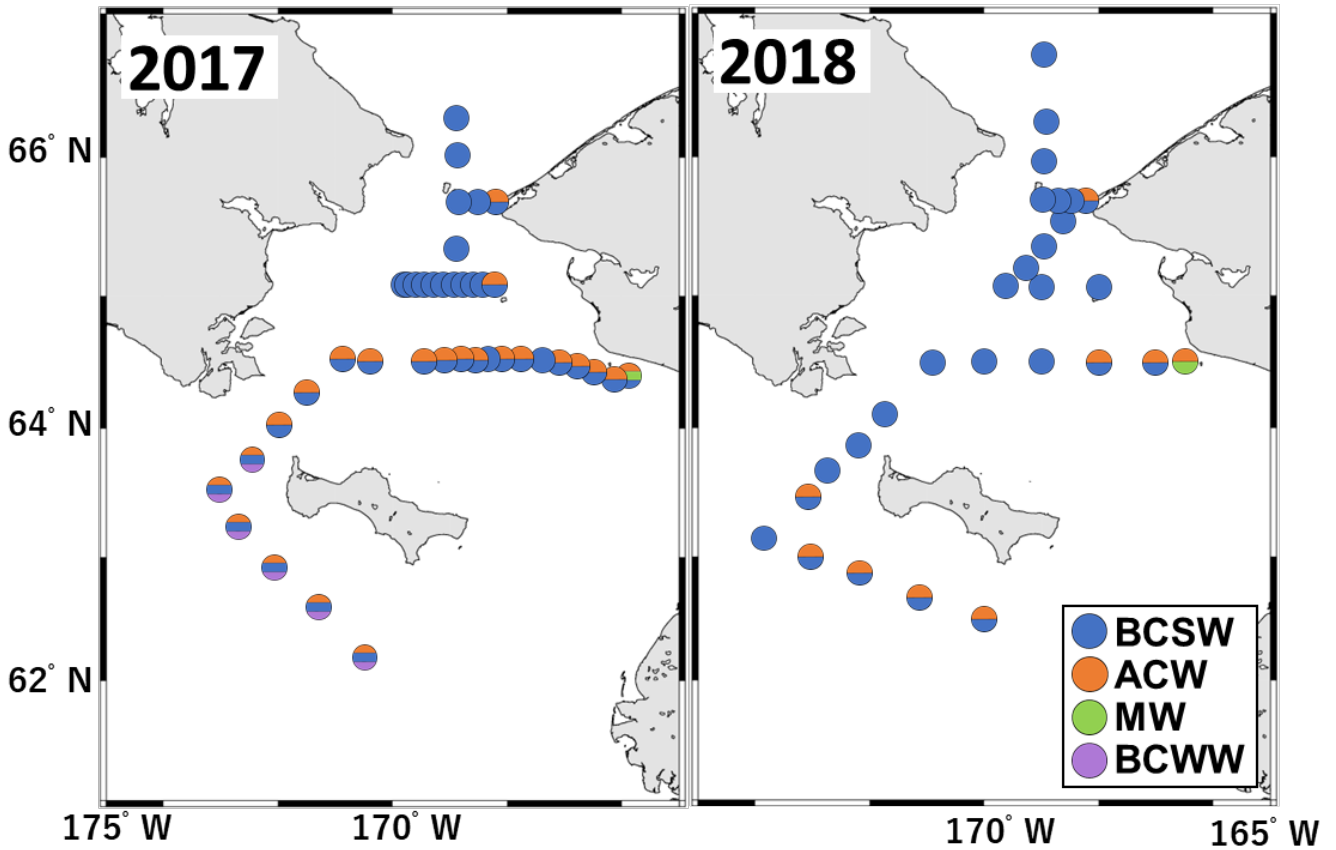


Fig. 4. Spatial distribution of water masses as defined by Danielson et al. (2017). BCSW: Bering-Chukchi Summer Water, ACW: Alaskan Coastal Water, MW: Melting Water, and BCWW: Bering-Chukchi Winter Water.

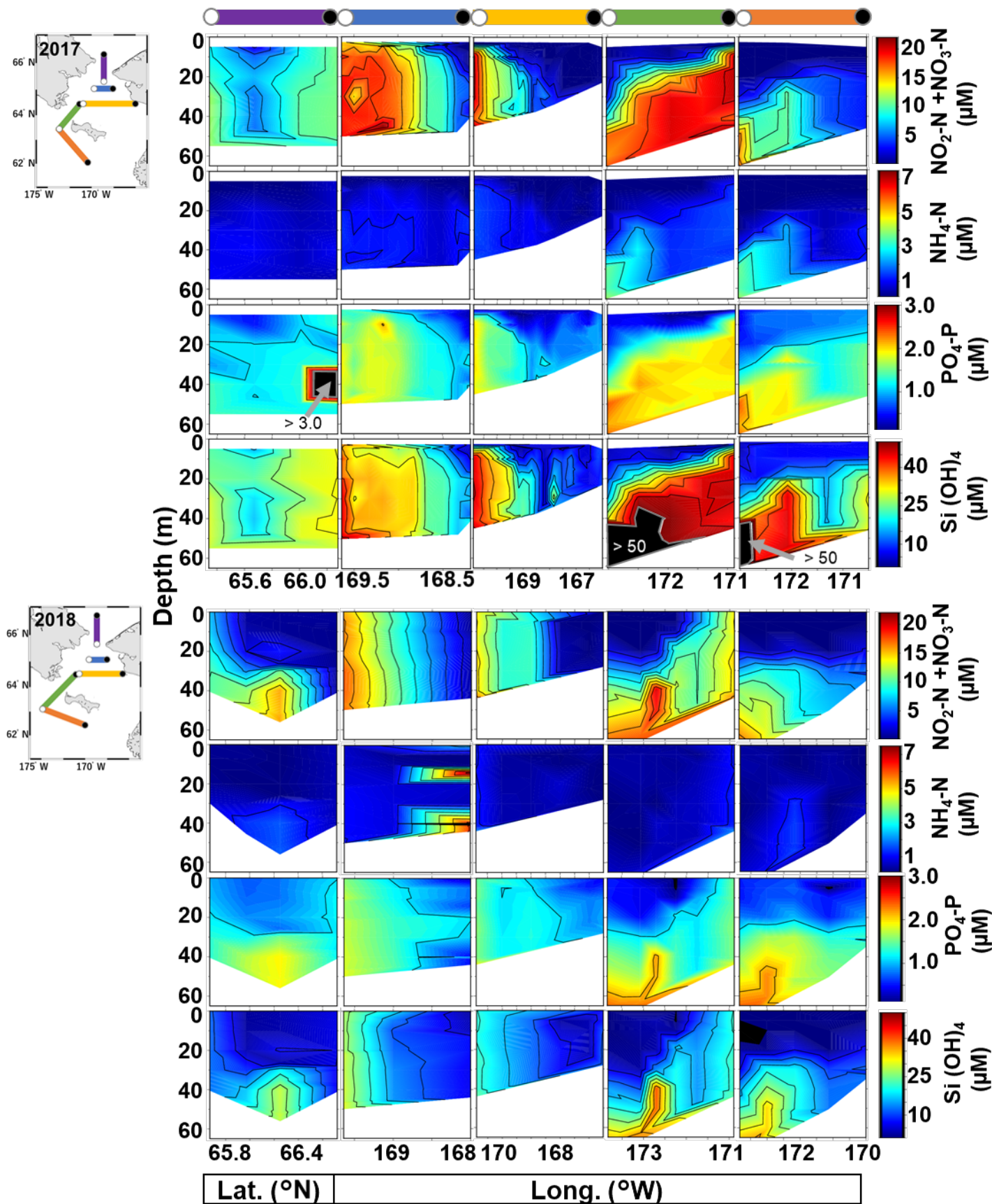


Fig. 5. Cross-sectional distributions of nutrient ( $\text{NO}_2\text{-N} + \text{NO}_3\text{-N}$ ,  $\text{NH}_4\text{-N}$ ,  $\text{PO}_4\text{-P}$ , and  $\text{Si(OH)}_4$ ) concentrations in the northern Bering Sea in 2017 (upper) and 2018 (lower).

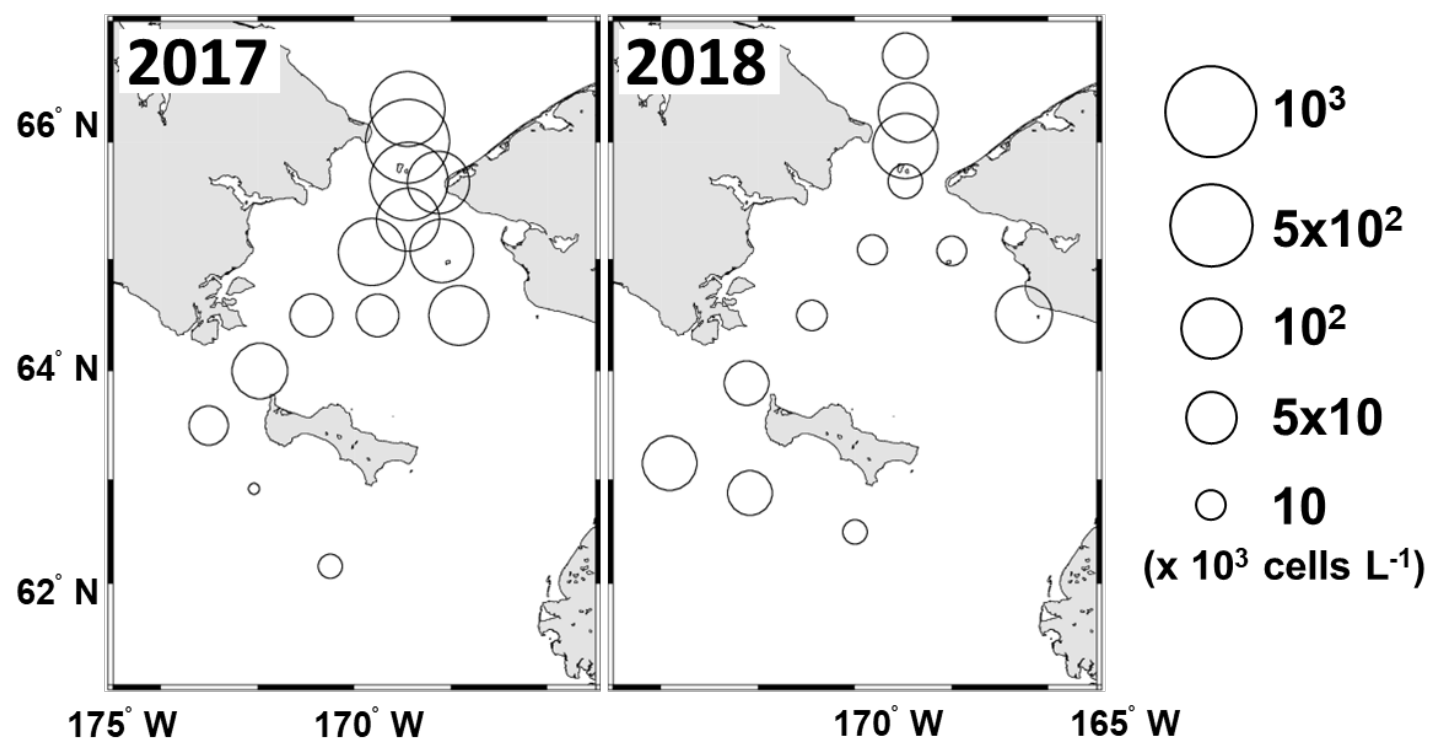


Fig. 6. Horizontal distribution of the average phytoplankton cell density in 2017 (left) and 2018 (right). The circles indicate the mean cell density in the water column.

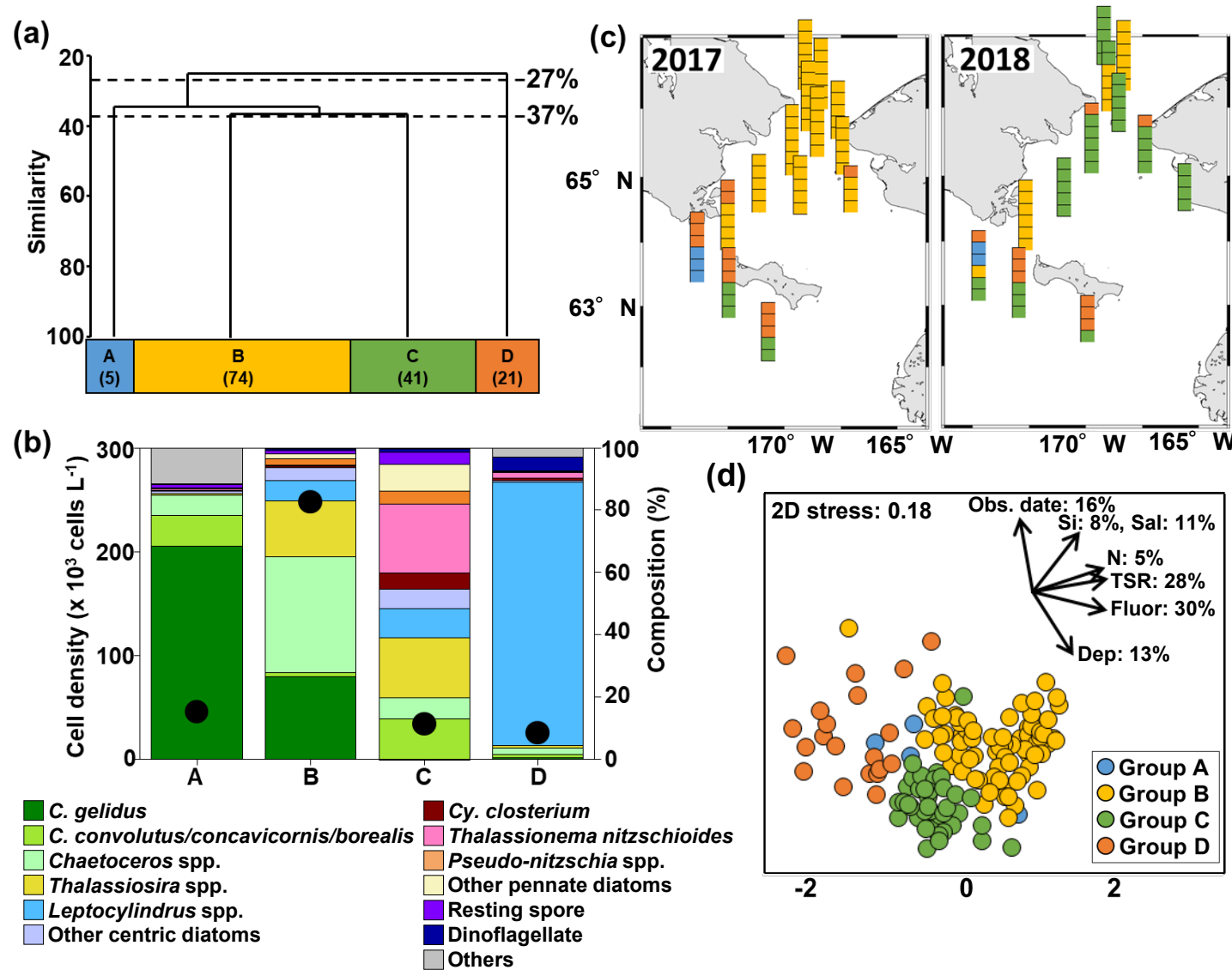
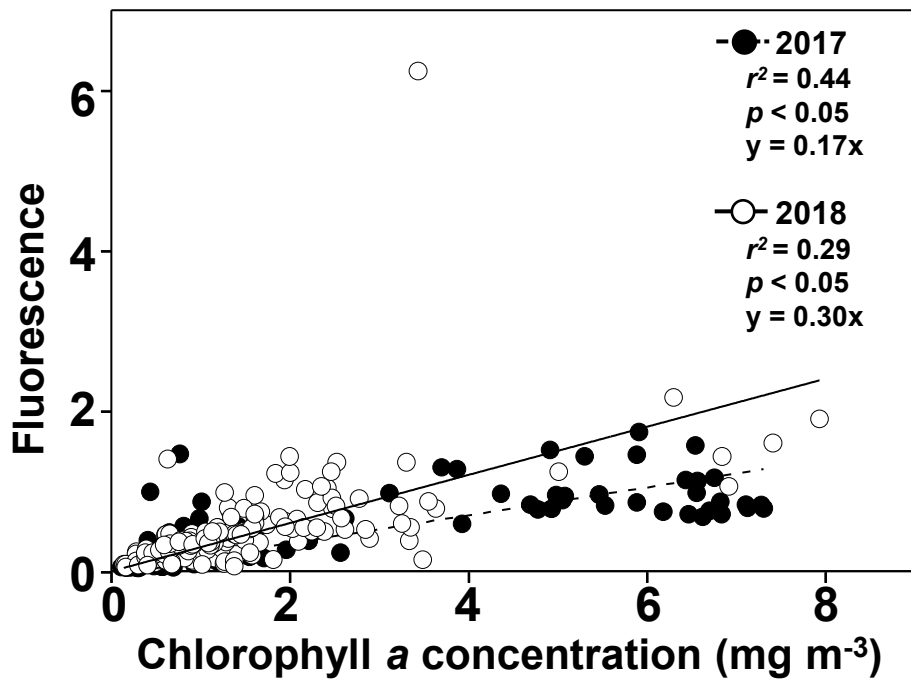
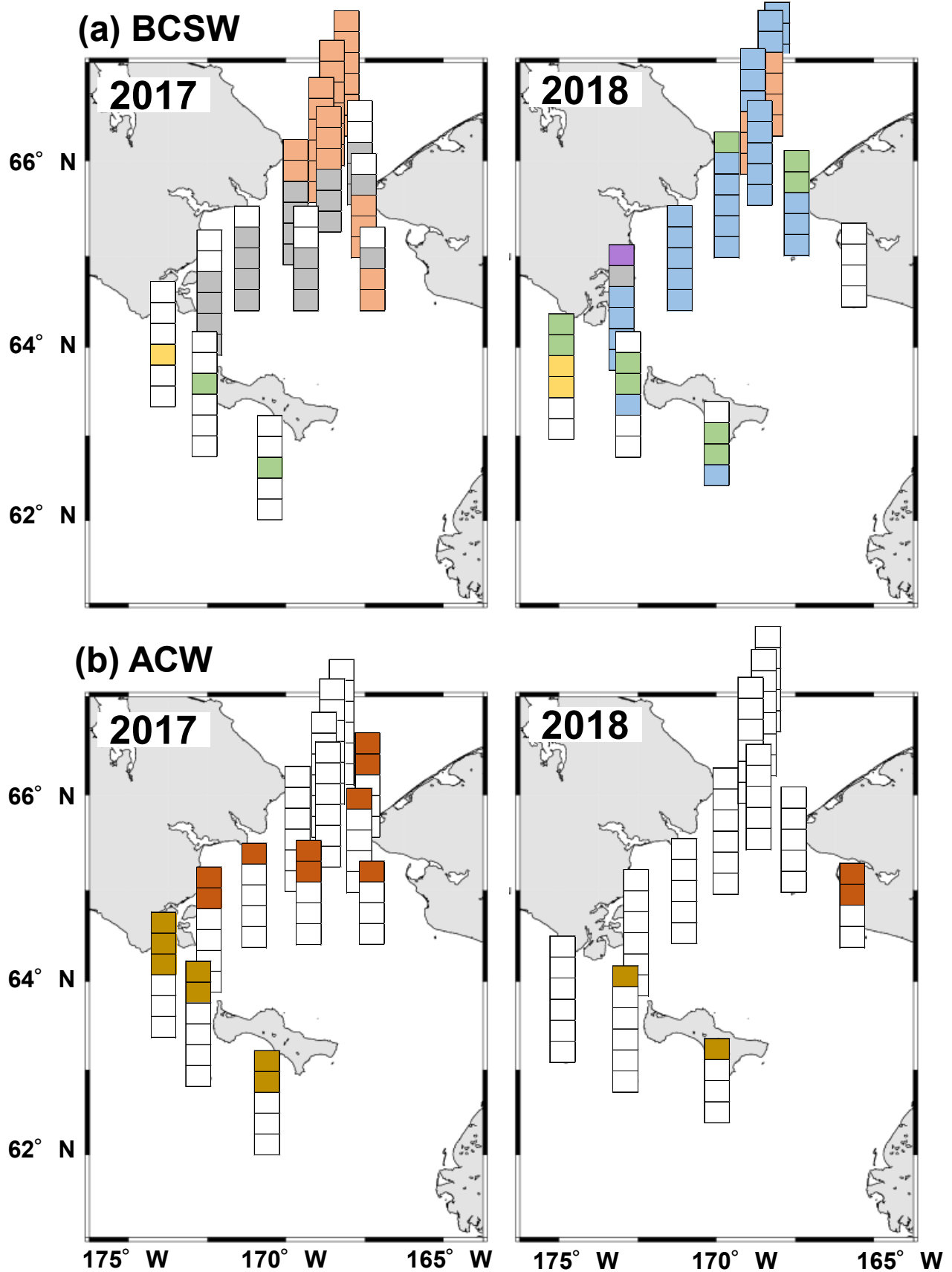


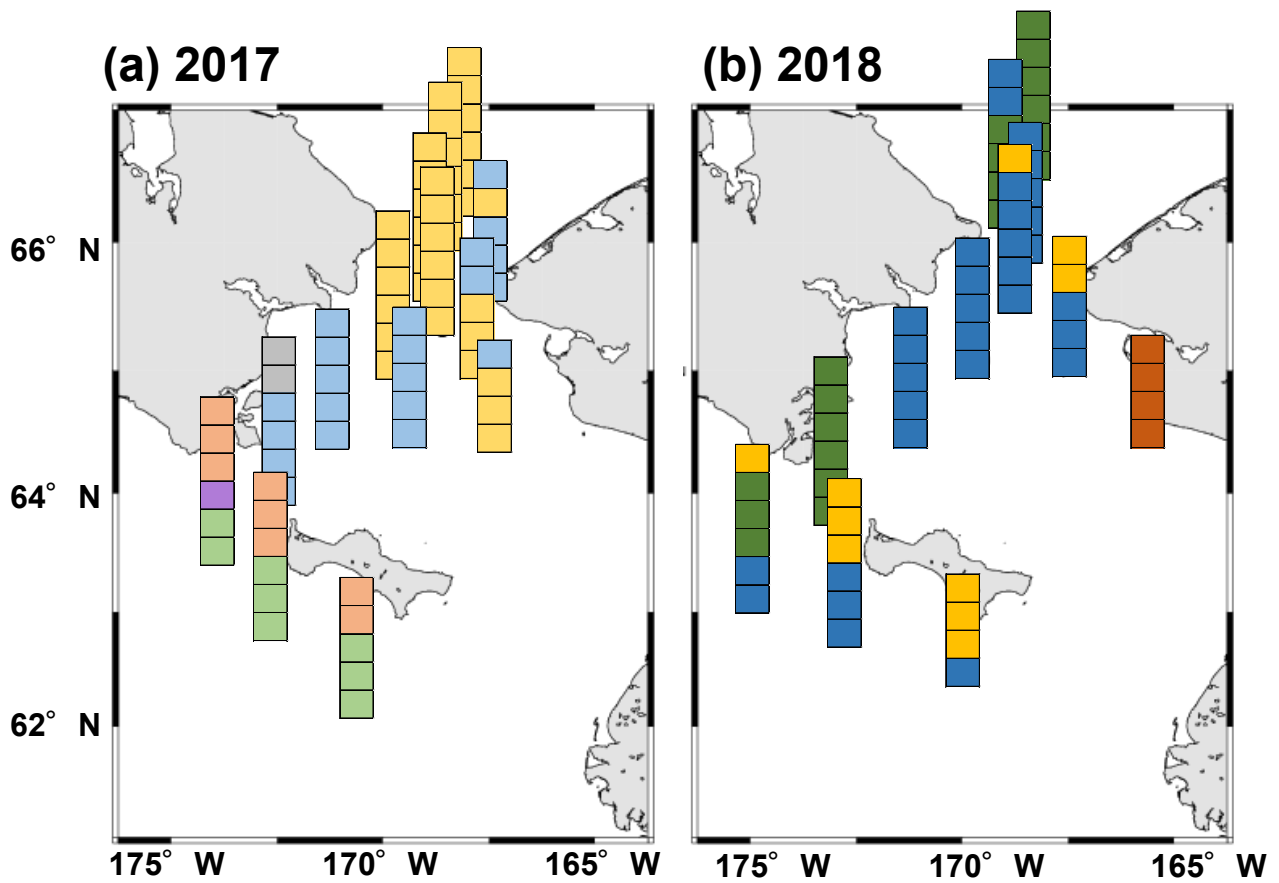
Fig. 7. (a) Results of the cluster analysis based on the phytoplankton cell density found by Bray-Curtis similarity. (b) Species composition and cell density of each group. (c) Spatial distribution of the phytoplankton community in the northern Bering Sea during the summers of 2017 (left) and 2018 (right). (d) Nonmetric multidimensional scaling plots of the four groups, with *arrows* and *percentages* indicating the directions of the environmental parameters and the coefficient of determination ( $r^2$ ), respectively. *Obs. date*: observation date, *Si*: silicate, *Sal*: salinity, *N*: nitrate and nitrite, *TSR*: the timing of sea ice retreat, *Fluor*: fluorescence, and *Dep*: sampling depth.



Appendix Fig 1. Relationship between the chlorophyll *a* concentration and the fluorescence.



Appendix Fig 2. Spatial distribution of the phytoplankton communities in each water mass (the BCSW (a) and the ACW (b)) by cluster analyses. The cluster analyses were conducted in each water mass independently. White boxes indicated water masses that were not the focus of this analysis. Color codes for the communities were shown different groups analyzed by the cluster analysis.



Appendix Fig 3. Spatial distribution of the phytoplankton communities in each year. Cluster analyses were conducted in each year independently. Color codes for the communities were shown different groups analyzed by the cluster analysis.